Family-wide analysis of integrin structures predicted by AlphaFold2

Heng Zhang[1], Daniel S. Zhu[1], and Jieqing Zhu[1,2] *

[1]Versiti Blood Research Institute, Milwaukee, WI, USA.

[2]Department of Biochemistry, Medical College of Wisconsin, Milwaukee, WI, USA.

*Corresponding author. Email: Jieqing.Zhu@versiti.org

Abstract

Recent advances in protein structure prediction using AlphaFold2, known for its high efficiency and accuracy, have opened new avenues for comprehensive analysis of all structures within a single protein family. In this study, we evaluated the capabilities of AphaFold2 in analyzing integrin structures. Integrins are heterodimeric cell surface receptors composed of a combination of 18 α and 8 β subunits, resulting in a family of 24 different members. Both α and β subunits consist of a large extracellular domain, a short transmembrane domain, and typically, a short cytoplasmic tail. Integrins play a pivotal role in a wide range of cellular functions by recognizing diverse ligands. Despite significant advances in integrin structural studies in recent decades, high-resolution structures have only been determined for a limited subsets of integrin members, thus limiting our understanding of the entire integrin family. Here, we first analyzed the single-chain structures of 18 α and 8 β integrins in the AlphaFold2 protein structure database. We then employed the newly developed AlphaFold2-multimer program to predict the α/β heterodimer structures of all 24 human integrins. The predicted structures show a high level of accuracy for the subdomains of both α and β subunits, offering high-resolution structure insights for all integrin heterodimers. Our comprehensive structural analysis of the entire integrin family unveils a potentially diverse range of conformations among the 24 members, providing a valuable structure database for studies related to integrin structure and function. We further discussed the potential applications and limitations of the AlphaFold2-derived integrin structures.

1. Introduction

Integrins are cell surface receptors that recognize a variety of extracellular or cell surface ligands, enabling communication between the cell's interior and exterior [1]. The human integrin family consists of 24 members, formed through the combination of 18 α and 8 β subunits (**Fig. 1**). These 24 α/β integrin heterodimers are either widely distributed or specifically expressed in particular cell types. As a result, they serve universal or specialized functions in cellular processes related to cell adhesion and migration. Based on ligand or cell specificity, integrins can be categorized into subfamilies, including RGD (Arg-Gly-Asp) receptors, collagen receptors, laminin receptors, and leukocyte-specific receptors [1]. Integrins play pivotal roles in various diseases such as thrombosis, inflammation, and cancer, rendering them attractive therapeutic targets by small molecule or antibody inhibitors [2-4]. Since their discovery in the early 1980s, research into integrin structure and function has been a continuous area of interest [5].

The α and β subunits of integrin are composed of multiple subdomains. The α subunit contains β-propeller, thigh, calf-1, calf-2, transmembrane (TM), and cytoplasmic tail (CT) domains (**Fig. 1A-C**). The β subunit comprises βI, hybrid, PSI, I-EGF 1-4, β-tail, TM, and CT domains (**Fig. 1A-C**). A subclass of α integrins has an extra αI domain inserted into the β-propeller domain (**Fig.1D-F**). In integrins without the αI domain, the α β-propeller and β βI domains combine to form the ligand binding site (**Fig. 1A-C**). In contrast, for αI-containing integrins, the αI domain is responsible for ligand binding (**Fig. 1D-F**). Integrin ectodomains can also be divided into the headpiece (containing the head and upper legs) and lower leg domains (**Fig. 1C**). In the past few decades, structural studies of integrins have unveiled a conformation-dependent activation and ligand binding mechanism, involving transitions among at least three conformational states [6,7]. The bent conformation with closed headpiece represents the resting state of integrin (**Fig. 1A, D**), while the extended closed headpiece and extended open headpiece represent the intermediate and high-affinity active states, respectively (**Fig. 1B-C, E-F**). The conformational transition of integrin can be initiated by the binding of intracellular activators, including talin and kindlin, to β CT, leading to inside-out signaling, or by the binding of extracellular ligands, resulting in outside-in signaling (**Fig. 1A-F**) [8, 9]. However, it's worth noting that the conformation-dependent activation model was primarily derived from structural studies of the highly-regulated β_2 and β_3 integrins, primarily expressed in blood cells [6,7]. Given the limited structural information available for most integrin members, it remains uncertain whether the current model of integrin conformational changes can be applied to the entire integrin family.

Since the publication of the first high-resolution crystal structure of the $\alpha_V\beta_3$ ectodomain in 2001 [10], substantial efforts have been dedicated to determining integrin structures using a variety of methods, including crystallography, negative-stain electron microscopy (EM), nuclear magnetic resonance (NMR), and more recently, cryogenic EM (cryo-EM). However, high-resolution structure information remains limited to only a few integrin members, including $\alpha_V\beta_3$ [10-12],[10-12] $\alpha_{IIb}\beta_3$ [13-21],[13-21] $\alpha_5\beta_1$ [22-24],[22-24] $\alpha_6\beta_1$ [25],[25] $\alpha_X\beta_2$ [26,27], $\alpha_L\beta_2$ [28], $\alpha_M\beta_2$ [29,30], $\alpha_V\beta_6$ [31-33], $\alpha_V\beta_8$ [34-37], and $\alpha_4\beta_7$ [38],

many of which have only had the fragment structures determined to date. Among the 24 integrins, the heterodimer structures of transmembrane-cytoplasmic (TM-CT) portion have been experimentally determined only for $\alpha_{IIb}\beta_3$ [20,39-43]. The recent breakthrough in protein structure prediction using the artificial intelligence-based AlphaFold2 program has provided a powerful tool for analyzing previously challenging-to-determine protein structures with a remarkable level of accuracy [44]. We conducted an analysis of the predicted atomic structure models of single-chain 18 α and 8 β integrins that are available in the AlphaFold2 database (**Fig. 1G**). Moreover, using the recently developed AlphaFold2-multimer program [45], we predicted the structures of all 24 human integrin α/β heterodimers. Our structural analysis of the entire integrin family revealed potential conformational diversity across its 24 members, with the identification of previously unknown structural features. Our study compiled a comprehensive database of integrin structures that can serve as a valuable resource for guiding functional and structural studies. Despite the limitations of predicted structures, these findings underscore the efficacy of AlphaFold2 in the family-wide structure prediction of large and complex proteins.

2. Materials and methods

2.1. Databases and software

The single-chain structures of 18 α and 8 β integrin subunits were downloaded from the AlphaFold2 database (https://alphafold.ebi.ac.uk). Human integrin protein sequences were downloaded from the NCBI protein database (https://www.ncbi.nlm.nih.gov/protein/). Experimentally determined structures, including $\alpha_{IIb}\beta_3$ (PDB 3FCS), $\alpha_V\beta_3$ (PDB 4G1E), $\alpha_5\beta_1$ (PDB 7NXD), and $\alpha_X\beta_2$ (PDB 4NEH), were downloaded from protein databank https://www.rcsb.org. All integrin structures were analyzed using PyMOL version 2.5.4 (The PyMOL Molecular Graphics System, Version 2.0 Schrödinger, LLC).

2.2. Running AlphaFold2

AlphaFold2 Version 2.1.2 was running on the HPC Cluster at the Medical College of Wisconsin using Miniconda3 virtual environments. The AlphaFold2 downloaded reference files are located at: “/hpc/refdata/alphafold”. Customized sbatch job script was submitted for structure prediction, shown as below.

```
#!/bin/bash
#SBATCH --job-name=alphafold_test
#SBATCH --ntasks=8
#SBATCH --mem=100gb
#SBATCH --time=48:00:00
#SBATCH --output=%x-%j.out
#SBATCH --gres=gpu:1
#SBATCH --partition=gpu
#SBATCH --partition=bigmem
```

```
module load alphafold/2.1.2

export NVIDIA_VISIBLE_DEVICES=$CUDA_VISIBLE_DEVICES
run_alphafold.sh -d $DOWNLOAD_DIR -f
/scratch/…/alphatest/integrin_heterodimer_amino_acid_sequence.fasta -t 2023-01-01 -o
/scratch/…/alphatest/  -m multimer
```

Typically, one GPU (--gres=gpu:1) and 100 GB memory (--mem=100gb) was requested to run AlphaFold2. The maximum job running time was set to 48 h (--time=48:00:00). To run AlphaFold2-Multimer for structure prediction of integrin heterodimers, an input fasta file containing the sequences of both integrin α and β subunits was provided. The multimer prediction function was enabled with command "--model_preset (-m)=multimer". Full length or extracellular domain structures of integrin heterodimers without signal peptides were predicted with or without templates by setting the parameter of "--max_template_date(-t)=2000-05-14" or "--max_template_date(-t)=2023-01-01". For integrin $\alpha_6\beta_4$ structure prediction, the large cytoplasmic tail of β_4 was truncated after KGRDV to simplify the prediction. The top ranked models were selected for further analysis.

2.3. Comparison of AlphaFold2 predicted integrin structures

The single chain α integrin structures downloaded from AlphaFold2 database were superimposed based on the α_{IIb} calf-2 domain using the "super" command in PyMOL. The single chain β integrin structures downloaded from AlphaFold2 database were superimposed based on the β_3 βI domain using the super command in PyMOL. The experimentally determined structures for α_{IIb} (PDB 3FCS), α_V (PDB 4G1E), α_5 (PDB 7NXD), and α_X (PDB 4NEH) were superimposed onto the predicted corresponding structures. The experimentally determined structures for β_3 (PDB 3FCS), β_1 (PDB 7NXD), and β_2 (PDB 4NEH) were superimposed onto the predicted structures accordingly. The integrin heterodimer structures predicted by AlphaFold2-multimer with or without TM-CT domains were superimposed onto the calf-2 domain of α_{IIb} in PyMOL. For structure comparison of integrin TM-CT heterodimers, the structures were superimposed based on the α_{IIb} TM domain. The aligned structures were individually oriented to position them perpendicularly to the cell membrane.

2.4. DNA constructs

The α_5 with C-terminal EGFP tag (α_5-EGFP) was a gift from Rick Horwitz (Addgene plasmid #15238; http://n2t.net/addgene:15238; RRID:Addgene_15238) [46]. The α_9 with C-terminal EGFP tag (α_9-EGFP) was a gift from Dean Sheppard (Addgene plasmid #13600; http://n2t.net/addgene:13600; RRID:Addgene_13600). The α_3, α_7, and α_{10} integrins were cloned into pEGFP-N3 vector using the SalI and KpnI restriction sites following the standard molecular cloning protocol. A pair of primers were designed for introducing N839Q mutation into the α_{10}-EGFP plasmid, forward primer: 5' gaacagaaaggaaaatgcttaccagacgagcctgagtctcatcttc 3'; reverse primer: 5' gaagatgagactcaggctcgtctggtaagcattttcctttctgttc 3'. The α_{10}-N839Q mutation was generated by QuickChange mutagenesis kit following the instruction (cat# 200517-5,

Agilent Technologies, Inc.). All DNA constructs were identified by sanger sequencing service provided by Retrogen, Inc.

2.5. Flow Cytometry Analysis of LIBS (Ligand Induced Binding Site) mAb binding

The LIBS rat mAb 9EG7 (cat# 553715, BD Biosciences) was used to measure the conformational extension of β_1 integrin. The mouse mAb MAR4 (cat# 555442, BD Biosciences) was used to measure total surface expression of β_1 integrin. The HEK293T cells were grown in complete DMEM (cat# 10-017-CV, Corning) supplemented with 10% fetal bovine serum (FBS) (cat# F2442, Sigma-Aldrich). Cells were maintained in a 37°C incubator with 5% CO_2. Flow cytometry analysis of integrin expression and LIBS mAb binding were as described previously [47]. In brief, HEK293T cells were transfected with EGFP-tagged α integrin constructs plus β_1 integrin. 48 hours post-transfection, the cells were detached, washed, and resuspended in HBSGB buffer (25 mM HEPES pH 7.4, 150 mM NaCl, 2.75 mM glucose, 0.5% BSA) containing 1 mM Ca^{2+}/Mg^{2+} or 0.1 mM Ca^{2+} plus 2 mM Mn^{2+}. Cells were incubated with 5 µg/ml of either 9EG7 mAb or MAR4 for 15 mins, followed by additional 15 min incubation with 10 µg/ml Alexa Fluor 647-conjugated goat anti-rat IgG (cat# A-21247, Invitrogen) or goat anti-mouse IgG (cat # A-21235, Invitrogen). Surface binding of mAb was measured by a BD Accuri™ C6 (BD Biosciences). The results were presented as a normalized mean fluorescence intensity (MFI) by calculating the MFI of 9EG7 binding (recognizing extended β_1) as a percentage of the MFI of MAR4 binding (recognizing total β_1). The plot was generated with Prism 9 software.

2.6. Data availability

The datasets generated during and/or analyzed during the current study are available from the corresponding author on reasonable request. A PyMol session file, named as “integrin-alphafold2-structure.pse”, that includes the predicted structures of integrin heterodimers were deposited online as supplementary materials.

3. Results

3.1. The AlphaFold2 single-chain structures of 18 α and 8 β human integrins

We extracted the structures of 18 human α integrins from the AlphaFold2 protein structure database. These integrin structure models in the AlphaFold2 database were predicted based on the full-length single-chain amino acid sequence, encompassing the signal peptide, ectodomain, TM and CT domains (**Fig. 1G**). The predicted models showed high accuracy in the domain structures, as indicated by the high score of predicted local distance difference test (pLDDT) (**Fig. 1G**). To compare the overall conformation of α integrin ectodomains, we superimposed all structures onto the calf-2 domain of α_{IIb}, vertically oriented them relative to the cell membrane, and adjusted their rotations to display the position of the β-propeller domain relative to the membrane (**Fig. 2**). We also superimposed the AlphaFold2 structures with the experimental structures of

α_{IIb}, α_V, α_5, and α_X. The structures were grouped based on ligand or cell specificity. Among the RGD-binding α integrins, α_{IIb} and α_V displayed a sharp bent conformation, nearly identical to their crystal structures (**Fig. 2A**). However, the α_5 AlphaFold2 structure exhibited a more bent conformation than its half-bent cryo-EM structure (**Fig. 2A)**. Among the three laminin receptors, only α_6 adopted a sharp bent conformation like the RGD receptors, while α_3 and α_7 showed a half-bent conformation (**Fig. 2B**). The α_4 and α_9 integrins also adopted a bent conformation similar to the RGD receptors (**Fig. 2C**). Interestingly, all four α integrins of collagen receptors exhibited more extended conformation than bent, with α_{10} in a nearly fully extended conformation (**Fig. 2D**). The five leukocyte-specific α integrins displayed conformational diversity, with α_L and α_X being more bent than α_M, α_D, and α_E (**Fig. 2E**). The AlphaFold2 structure of α_X closely resembled the α_X crystal structure (**Fig. 2E**).

We next analyzed the structures of 8 human β integrins, all of which were predicted as single-chain structures in the AlphaFold2 database. The predicted domain structures of β integrins also exhibit a high level of accuracy, as indicated by the pLDDT score (**Fig. 1G**). To compare the overall conformation, we superimposed the structures based on the β_3 βI domain, and then individually orientated them vertically to membrane normal. We also superimposed the AlphaFold2 structures with the experimental structures of β_1, β_2 and β_3. As depicted in **Fig. 3**, the individual domains, including βI, PSI, hybrid, I-EGF domains, and β-tail domain (β-TD), were accurately predicted for β_1 to β_7 integrins. However, the β-TD of β_8 appeared smaller than other β integrins, and its structure was incompletely predicted (**Fig. 3, β_8**). The AlphaFold2 structures of β_3, β_2, β_4, β_5, β_6, and β_7 all adopted a bent conformation as seen in the crystal structures of β_3 and β_2, whereas the β_1 and β_8 structures exhibited less bending (**Fig. 3**). The half-bent conformation of β_1 AlphaFold2 structure closely resembled the cryo-EM structure (**Fig. 3, β_1**).

3.2. The domain interface where α and β integrin subunits undergo extension

Previous structural studies have revealed that the extension of α integrin occurs at the interface between the thigh and calf-1 domains, where a disulfide bonded knob, known as the genu, is located (**Fig. 1C, F**). We conducted a sequence alignment of all α integrins at the junction between the thigh and calf-1 domains (**Fig. 4A**). To illustrate the interface between the thigh and calf-1 domains in a bent conformation, we used the structure of α_{IIb} as an example (**Fig. 4B**). Interfacial residues are highlighted in red in the sequence alignment (**Fig. 4A**) and shown as red sticks in the structure (**Fig. 4B**). The sequence alignment reveals that the interfacial residues, as well as the putative N-glycan sites, are not highly conserved (**Fig. 4A**). Some α integrins, such as α_V, α_8, α_4, α_9, α_{10}, and α_E, contain putative N-glycan sites at the interface of either thigh or calf-1 domains. Interestingly, the laminin receptors α_3, α_6, and α_7 all have a longer interfacial loop (region 1) on the calf-1 domain (**Fig. 4A**). However, no signature sequences appear to indicate a preference for a bent or extended conformation.

The integrin β subunit extends at the junction between I-EGF-1 and I-EGF-2 (**Fig. 1C, F**). Sequence alignment of the eight human β integrins in this region showed no obvious

residue conservation, except for the typical disulfide bonds of EGF domains (**Fig. 4C**). In the bent conformation of β_3 integrin (**Fig. 4D**), the interface between I-EGF-1 and I-EGF-2 is considerably smaller compared to the interface between the thigh and calf-1 in α_{IIb} (**Fig. 4B**), suggesting that it is unlikely to play a major role in maintaining the bent structure. However, the length of C1-C2 loop in I-EGF-2 domain has been shown to regulate integrin extension [48]. Notably, a landmark disulfide bond is absent in the I-EGF-1 domain of β_8 (**Fig. 4C**), which may contribute, at least in part, to the distinct conformational regulation of β_8 integrin.

3.3. α_{10} integrin prefers an extended conformation on cell surface

Among the 18 α integrins, the AlphaFold2 structure of α_{10} reveals an extended conformation (**Fig. 2D**). This extended structure was also observed in α_{10} from other species, such as mouse, rat, and zebrafish (**Fig. 5A**). Notably, we identified a conserved putative N-glycan site (N839 in human) at the interface between the thigh and calf-1 domains of α_{10} integrin (**Fig. 5A**). It is plausible that N-glycans at this site may interfere with the bent conformation (**Fig. 5B**).

It is important to note that α_{10} integrin only forms heterodimer with β_1 integrin. The AlphaFold2 structures of human, mouse, cat, and chicken β_1 integrins all exhibit a half-bent conformation (**Fig. 5C**). To measure the conformation of $\alpha_{10}\beta_1$ on cell surface, we used mAb 9EG7, which recognizes the β_1 I-EGF-2 epitope that remains concealed in the bent conformation (**Fig. 5C**) [49]. This antibody reports on β_1 integrin extension. As a positive control, we used the universal integrin activator Mn^{2+} to induce integrin extension. For comparison with α_{10}, we selected α_3, α_5, α_7, and α_9 integrins.

In our experiments, α integrins were expressed as EGFP-fusion proteins alongside β_1 integrin in HEK293T cells. Flow cytometry analysis under physiological metal ion condition (1 mM Ca^{2+}/Mg^{2+}) revealed that α_{10}-EGFP/β_1 cells exhibited higher binding to 9EG7 compared to other integrins (**Fig. 5D**). Conversely, α_7-EGFP/β_1 and α_9-EGFP/β_1 cells showed increased 9EG7 binding only under the activating condition (0.1 mM Ca^{2+}/ 2 mM Mn^{2+}). In contrast, α_3-EGFP/β_1 cells did not response to Mn^{2+} (**Fig. 5D**). α_5-EGFP/β_1 cells also exhibited limited responsiveness to Mn^{2+} for 9EG7 binding compared to α_7 and α_9. However, the RGD-like compound MK-0429 effectively induced 9EG7 binding to α_5-EGFP/β_1 cells (**Fig. 5D**). Notably, Mn^{2+} did not further increase 9EG7 binding to α_{10}-EGFP/β_1 cells (**Fig. 5D**). Mutating the putative N-glycan site at the interface between the thigh and calf-1 domains of α_{10} integrin (α_{10}-N839Q) did not affect 9EG7 binding (**Fig. 5D**). These data suggest that α_{10} integrin maintains a constitutively extended conformation on cell surface.

3.4. The integrin α/β heterodimer structures predicted by AlphaFold2-multimer

Integrins are typically expressed as heterodimers on cell surface, consisting of both α and β subunits. However, the integrin structures in AlphaFold2 database were modeled individually for the single-chain α and β subunits, as described above. To construct integrin structures containing both α and β subunits, we utilized the AlphaFold2-

multimer module for structure prediction of all 24 human integrin heterodimers. To prevent potential model bias arising from the templates of experimental integrin structures, we set the template search date to the year 2000, predating the reporting of any integrin heterodimer structures. Impressively, AlphaFold2-multimer successfully predicted the structures of all 24 integrin heterodimers (**Fig. 6**). These structures were categorized based on their ligand or cell specificity. To facilitate conformational comparisons, all structures were superimposed onto the α_{IIb} calf-2 domain and individually orientated to align their ectodomains vertically with respect to the cell membrane (**Fig. 6**). Overall, the inter-subunit interfaces, including those of the α β-propeller and β βI domains, were accurately modeled. Notably, the AlphaFold2 structures of $\alpha_{IIb}\beta_3$ and $\alpha_V\beta_3$ ectodomains closely resembled their respective crystal structures, with a Cα root-mean-square deviation (RMSD) of approximately 2 Å, highlighting the outstanding capability of AlphaFold2 in modeling integrin structures. Among the RGD receptors, all adopted a bent conformation, except $\alpha_5\beta_1$, which exhibited a half-bent (**Fig. 6A**). Similarly, all laminin receptors, including $\alpha_7\beta_1$, displayed a bent conformation (**Fig. 6B**). Interestingly, the four collagen receptors, including $\alpha_{10}\beta_1$, exhibited a half-bent structure (**Fig. 6C**), in contrast to the AlphaFold2 structure of single-chain α_{10} showing a more extended conformation (**Fig. 2D**). Within the leukocyte-specific integrins, only $\alpha_L\beta_2$ and $\alpha_E\beta_7$ displayed a sharp bent conformation, while $\alpha_M\beta_2$, $\alpha_X\beta_2$, $\alpha_D\beta_2$, and $\alpha_E\beta_7$ appeared to be more extended (**Fig. 6D**). The AlphaFold2 structures of $\alpha_4\beta_1$ and $\alpha_9\beta_1$ showed a half-bent conformation (**Fig. 6E**). It is worth noting that the relative orientation of the TM domains to the cell membrane was not correctly predicted for most of the structures.

As nine of the integrin structures predicted by AlphaFold2-multimer show artificial interactions between TM-CT and ectodomains (**Fig. 7A**), we asked whether such interactions have any impact on the overall integrin structure prediction. We performed AlphaFold2-multimer modeling of the nine integrin structures in the absence of the TM-CT sequences. Surprisingly, the resulting structures closely matched those containing TM-CT domains (**Fig. 7B**), indicating that the structure modeling of the ectodomain and TM-CT domains does not influence each other during the structure calculation by AlphaFold2-multimer.

We proceeded to investigate whether the provision of structure templates to AlphaFold2-multimer had any impact on the calculation of integrin structures. For this test, we selected $\alpha_5\beta_1$, $\alpha_{10}\beta_1$, $\alpha_V\beta_8$, and $\alpha_X\beta_2$ integrins. The template searching date was set to the year 2023, which allowed AlphaFold2 to use the integrin crystal structures as templates during structure calculation. The results show that all four integrin structures calculated by AlphaFold2-multimer, denoted as $\alpha_5\beta_1$-2023, $\alpha_{10}\beta_1$-2023, $\alpha_V\beta_8$-2023, and $\alpha_X\beta_2$-2023, exhibited a sharp bent conformation (**Fig. 8A-D**), closely resembling the crystal structure of bent $\alpha_{IIb}\beta_3$ (**Fig. 8A**). For $\alpha_5\beta_1$ integrin, this contrasts with the half-bent structure predicted by AlphaFold2-multimer with a search date set at the year 2000, denoted as $\alpha_5\beta_1$-2000 (**Fig. 8A**). Indeed, the $\alpha_5\beta_1$-2000 structure closely resembles the $\alpha_5\beta_1$ cryo-EM structure (**Fig. 8A**). Similarly, the $\alpha_{10}\beta_1$-2023 structure showed a bent conformation compared to the half bent $\alpha_{10}\beta_1$-2000 structure (**Fig. 8B**). However, both $\alpha_V\beta_8$-2023 and $\alpha_V\beta_8$-2000 structures exhibited similar bent conformation (**Fig. 8C**). In

contrast, the $\alpha_X\beta_2$-2023 structure closely resembled the bent $\alpha_X\beta_2$ crystal structure, while the $\alpha_X\beta_2$-2000 structure appeared extended (**Fig. 8D**). These findings suggest that the inclusion of template structures can significantly influence the outcomes of structure prediction by AlphaFold2-multimer.

3.5. Structures of integrin TM-CT domains

Despite the apparent simplicity of the sequences and structures of integrin TM and CT domains, experimental structure determination has been limited to the $\alpha_{IIb}\beta_3$ TM-CT heterodimer. Through sequence alignment of the TM-CT domains from 8 β and 18 α human integrins, we identified conservative features at the TM, membrane-proximal (MP), and membrane-distal (MD) regions (**Fig. 9A**). These sequence conservative features were analyzed in the 24 integrin TM-CT structures calculated by AlphaFold2-multimer (**Fig. 9B**). Structure alignment revealed a high degree of structural similarity among the heterodimers at the TM domain, highlighting the conserved GXXXG motif in α and the conserved small G/A residue in β at the α/β TM interface (**Fig. 9B**). In the CT MP regions, the conserved GFFKR motif in the 18 α integrins all adopted a reverse turn conformation. The β CT MP regions, except for β_4 and β_8 integrins, displayed an α-helical structure extending from the TM α-helix, with the conserved Asp residue located at the α/β interface (**Fig. 9B**). The conserved β CT Asp residue is positioned proximal to the conserved Arg residue in the α GFFKR motif (**Fig. 9B**), which was proposed to form a salt bridge interaction [50]. The CT MD regions of both α and β subunits exhibited diverse disordered conformations, including the conserved NPXY motif responsible for binding talin (**Fig. 9B**). Despite not including any integrin TM-CT structure templates during the AlphaFold2-multimer calculation, the predicted $\alpha_{IIb}\beta_3$ TM-CT structure closely resembled the experimentally determined structure (**Fig. 9C**). Additionally, we performed AlphaFold2-multimer modeling for the $\alpha_{IIb}\beta_3$ TM-CT structure in the absence of the ectodomain, which showed a similar TM interface as the model generated along with the ectodomain (**Fig. 9D**). These results suggest that AlphaFold2-multimer is capable of accurately predicting integrin TM structures.

4. Discussion

Our AlphaFold2-assisted structural analysis of the entire integrin family demonstrated the high performance of AlphaFold2 in predicting integrin structures. Sequence alignment analysis revealed an average sequence identity of 30-40% among the 8 β integrins and 20-40% among the 18 α integrins [38]. For individual integrin domains, such as the βI domain, the sequence identity can exceed 60% [10-12]. Since AlphaFold2 incorporates amino acid sequences, multiple sequence alignments, and homologous structures in its structure calculation [44], the high sequence identity among integrin domains likely contribute to the accurate prediction of integrin domain structures for most family members. This accuracy is exemplified by the striking similarity between the predicted structures and the experimental structures of $\alpha_{IIb}\beta_3$, $\alpha_V\beta_3$, and $\alpha_X\beta_2$. Therefore, these predicted domain structures of integrins can be employed with a high level of confidence. They serve as valuable structural references

for delineating domain boundaries when constructing integrin proteins for structural and functional studies. Moreover, the high-resolution structural models can be used for mutagenesis studies, identifying putative N-glycan sites and antibody epitopes, and interpreting data from functional experiments.

In addition to accurately predicting integrin domain structures, AlphaFold2 successfully modeled the global conformations of integrins in bent, intermediate (half-bent), or extended states. Remarkably, AlphaFold2's calculations closely resembled the crystal structures for the bent conformations of α_{IIb}, α_V, α_X, β_2, and β_3 integrins. According to the current integrin activation model, integrin activation involves a structural transition from a bent to an extended conformation. It is not readily known whether the intermediate and extended conformations predicted by AlphaFold2 for certain integrins represent a resting or activating state. However, these models are valuable for generating structure-based hypotheses that can be experimentally tested. For example, AlphaFold2 predicted an extended conformation for the single-chain α_{10} structure and a half-bent conformation for the $\alpha_{10}\beta_1$ heterodimer. Consistent with these predictions, our flow cytometry assays, using mAb 9EG7 to report β_1 integrin extension, suggest a constitutive extended conformation of α_{10} in the resting condition on cell surface, which was not previously expected. Notably, the single-chain α_7 structure also exhibited an extended conformation, whereas the $\alpha_7\beta_1$ heterodimer was modeled in a bent conformation. The 9EG7 binding assay indicated that $\alpha_7\beta_1$ prefers a bent state under the resting condition on cell surface. However, the presence of activating Mn^{2+} induced more 9EG7 binding to $\alpha_7\beta_1$ compared to other integrins such as $\alpha_3\beta_1$ and $\alpha_9\beta_1$ that were predicted to be bent by AlphFold2, suggesting that α_7 integrin may be prone to becoming extended. These results imply that the overall integrin conformations predicted by AlphaFold2, especially for the underexplored integrins, can serve as reference structures for proposing functional assays.

AlphaFold2-multimer has demonstrated remarkable success in accurately predicting the structures of protein complexes, including those with transient interactions, multiple subunits, and large interfaces [51,52]. Here, we have shown that the AlphaFold2-multimer algorithm successfully predicts the structures of large complexes of integrin heterodimers. Furthermore, AlphaFold2 has exhibited excellent performance in predicting both fragment and full-length integrin structures. For instance, AlphaFold2-multimer's modeling of integrin ectodomains remains consistent regardless of the presence or absence of TM-CT domains. Similarly, AlphaFold2-multimer effectively modeled the heterodimeric structures of integrin TM-CT domains, even in the absence of the ectodomain. Additionally, AlphaFold2 modeling may capture the conformational heterogeneity and intrinsically disordered regions, as observed in the predicted structures of integrin cytoplasmic domains.

Despite its relatively high accuracy, the integrin structures predicted by AlphaFold2 have apparent limitations. Notably, these predictions do not incorporate glycan structures and essential metal ions, both of which are vital components for integrin structure and function. Furthermore, the relative orientation between ectodomain and TM-CT domains cannot be correctly modeled by AlphaFold2. Additionally, our

observations indicate that AlphaFold2-multimer predictions can be influenced by the homologous structures, potentially introducing bias when modeling the overall conformation of integrins. Therefore, we recommend conducting integrin structure calculations with AlphaFold2-multimer in the absence of template structures.

5. Conclusions

In summary, our family-wide structural analysis of integrins using AlphaFold2 showcases the remarkable capabilities of AlphaFold2 in modeling complex structures. The comprehensive structure database containing all 24 integrin heterodimers can be used as high-resolution structure resources for advancing both structural and functional studies within the integrin family.

Funding

This work was supported by the grant R01 HL131836 (to J. Zhu) from the Heart, Lung, and Blood Institute of the National Institute of Health.

Author contributions

Heng Zhang: Investigation, Visualization, Writing-Reviewing and Editing.
Daniel S. Zhu: Visualization, Writing-Reviewing and Editing.
Jieqing Zhu: Conceptualization, Supervision, Visualization, Funding acquisition, Writing-Original Draft preparation.

Declaration of Competing Interest

None declared.

Acknowledgement

We thank the Research Computing Center at the Medical College of Wisconsin for providing the help and resources in running the AlphaFold2 program.

Figures and legends

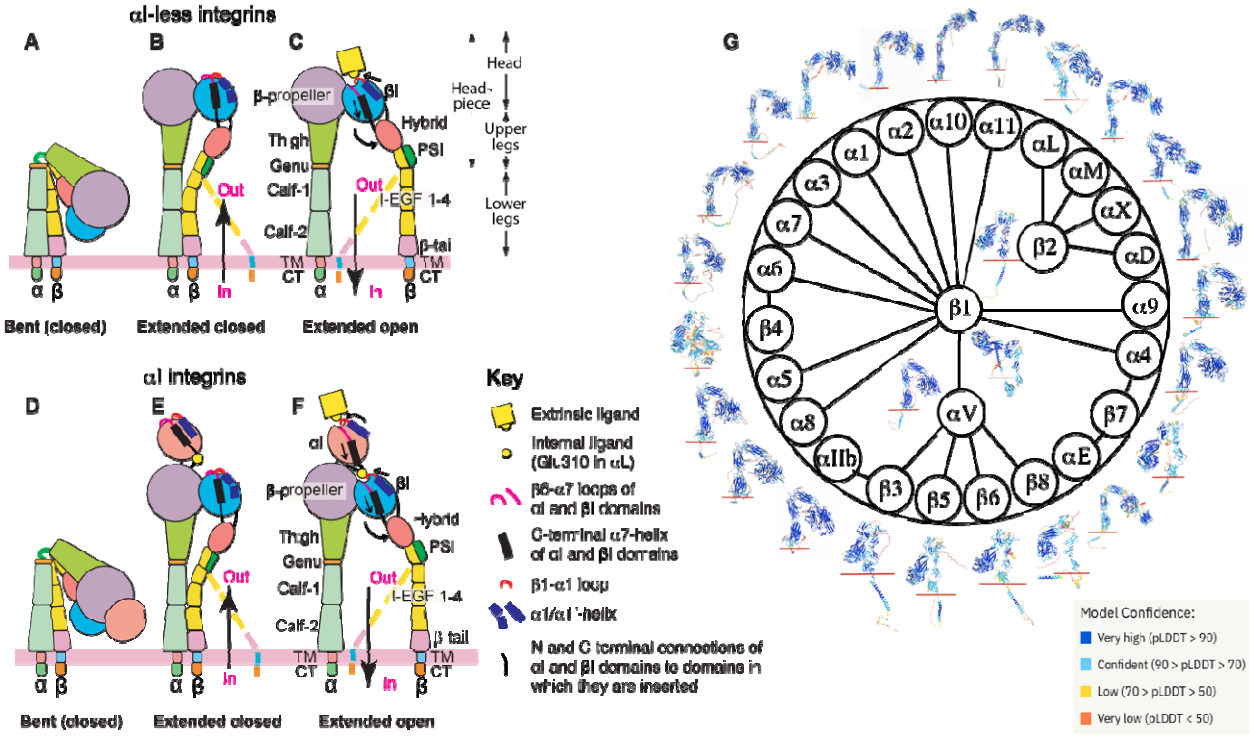

Figure 1. Integrin domain organization and structures predicted by AlphaFold2. (**A-F**) Integrin domain organization and conformational changes during activation are depicted for both αI-less (A-C) and αI-containing (D-F) integrins. The figures illustrate global and local structural changes, with dashed lines representing alternative conformations of the β leg domains. (**G**) The integrin family and overall structures of α and β subunits predicted by AlphaFold2 are displayed, with the red line marketing the boundary between the extracellular and transmembrane (TM) domains. The structure images are color-coded based on model confidence calculated as pLDDT scores.

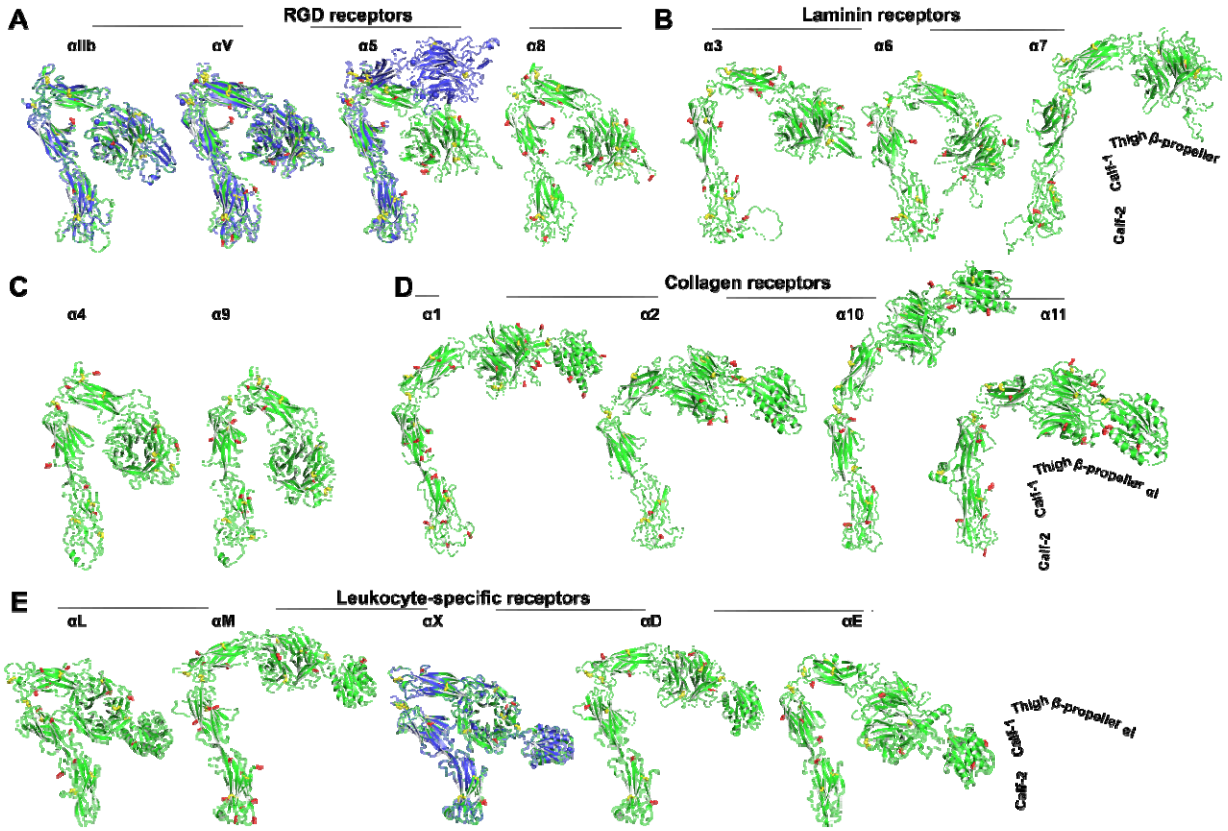

Figure 2. AlphaFold2 structures of the ectodomains of 18 human α integrins. The Alphafold2 structures are represented in green, while the experimentally determined structures for α_{IIb} (PDB 3FCS), α_V (PDB 4G1E), α_5 (PDB 7NXD), and α_X (PDB 4NEH) are displayed in blue. Red sticks indicate putative N-linked glycosylation sites, and yellow sticks represent disulfide bonds. The structures were aligned based on the calf-2 domain and are oriented perpendicularly to the cell membrane.

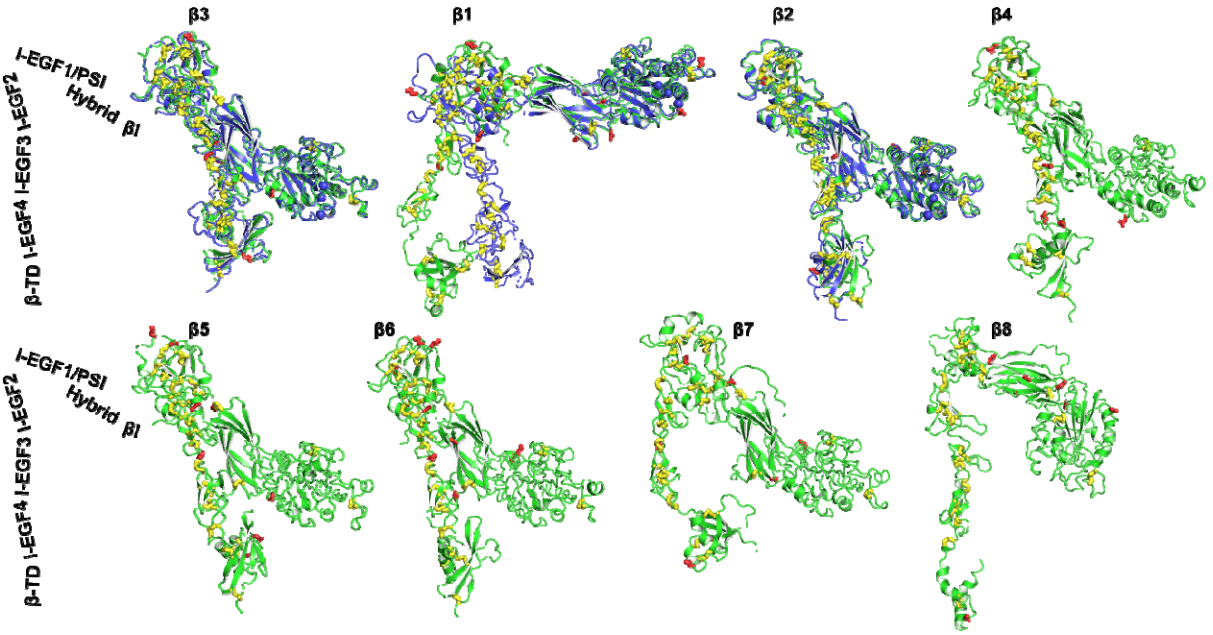

Figure 3. **AlphaFold2 structures of 8 human β integrins**. AlphaFold2 structures are depicted in green, while experimentally determined structures for β_3 (PDB 3FCS), β_1 (PDB 7NXD), and β_2 (PDB 4NEH) are shown in blue. The putative N-linked glycosylation sites are represented as red sticks, and disulfide bonds are shown as yellow sticks. The structures were aligned based on the β_3 βI domain and are oriented perpendicularly to the cell membrane.

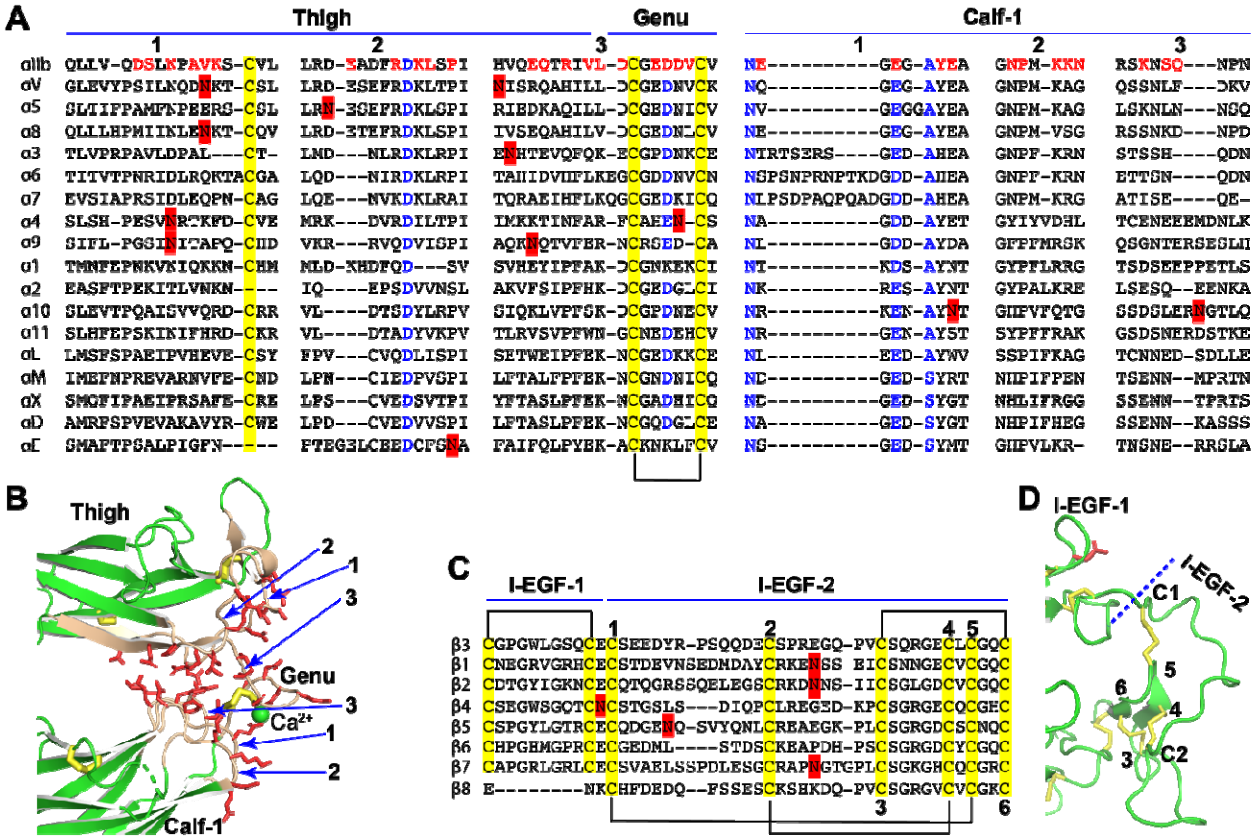

Figure 4. **Sequence and structure of the domain interface where integrin becomes extended**. (**A**) Sequence alignment of the human α integrin thigh and calf-1 domain junction interface. Interfacial residues of α_{IIb} are highlighted in red, while highly conserved residues are in blue. Disulfide bonds are indicated in yellow, and putative N-glycan sites are marked in red. (**B**) The interface between the thigh and calf-1 domains of the bent α_{IIb} structure. The loops at the interface are numbered in panels A and B. Interfacial residues are shown as red sticks. Disulfide bonds are represented by yellow sticks. (**C**) Sequence alignment of the human β integrin I-EGF-1 and I-EGF-2 domain junction. Disulfide bonds are highlighted in yellow and putative N-glycan sites are marked in red. The six cysteines of I-EGF-2 domain are numbered. (**D**) Structure of β_3 I-EGF-1 and I-EGF-2 domain junction. Disulfide bonds are shown as yellow sticks, and one N-glycan site on I-EGF-1 is depicted as a red stick.

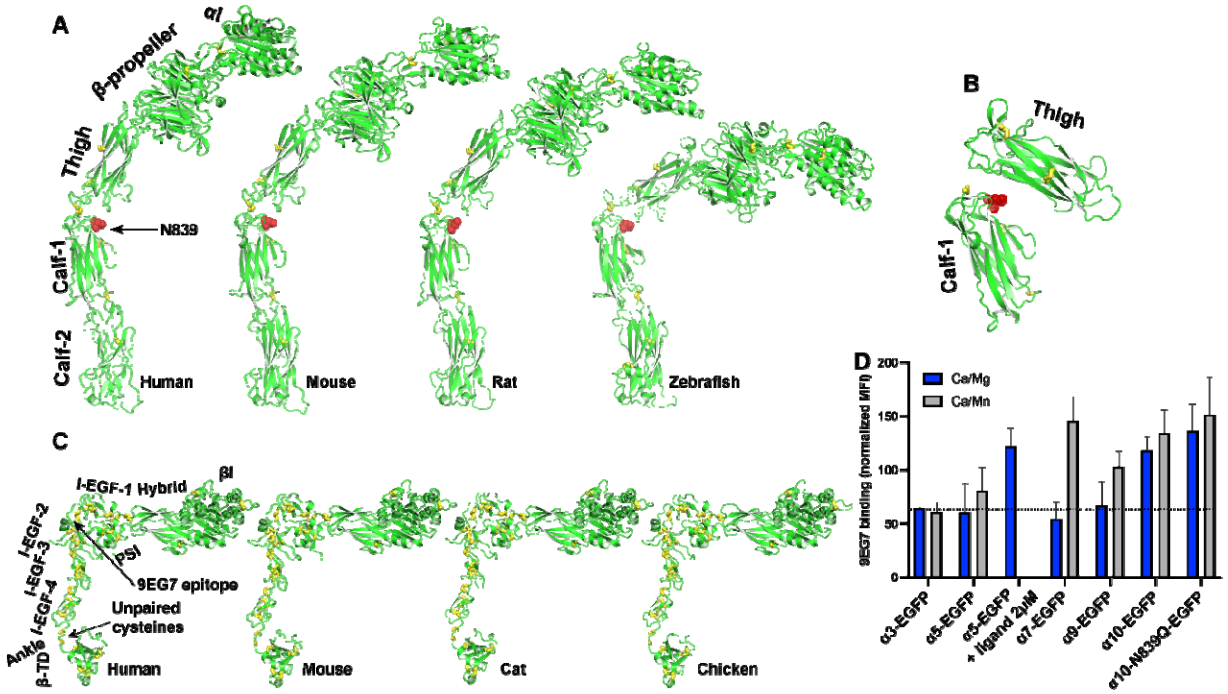

Figure 5. **AlphaFold2 structures of α_{10} and β_1 integrins from different species**. (**A**) Structures of α_{10} integrins from human, mouse, rat, and zebrafish. The structures were aligned based on the calf-2 domain and oriented perpendicularly to the cell membrane. The N-glycan site at the thigh/calf-1 interface is shown as a red stick. (**B**) Relative positions of α_{10} thigh and calf-1 domains in the fully bent conformation, illustrating the interfacial location of the N-glycan site shown as red sticks. The thigh and calf-1 domains of α_{10} were superimposed on those of bent α_{IIb} integrin structure. (**C**) Structures of β_1 integrins from human, mouse, cat, and chicken. The structures were aligned based on the βI domain and oriented perpendicularly to the cell membrane. (**D**) Conformation of β_1 integrin co-expressed with selected integrin α subunit. Human integrin α subunits with a C-terminal EGFP tag were co-expressed with human β_1 in 293T cells. The binding of mAb 9EG7 or MAR4 was measured by flow cytometry in a buffer containing 1 mM Ca^{2+}/Mg^{2+} or 0.1 mM Ca^{2+} plus 2 mM Mn^{2+}. The data are presented as the MFI of 9EG7 binding as a percentage of the MFI of MAR4 binding.

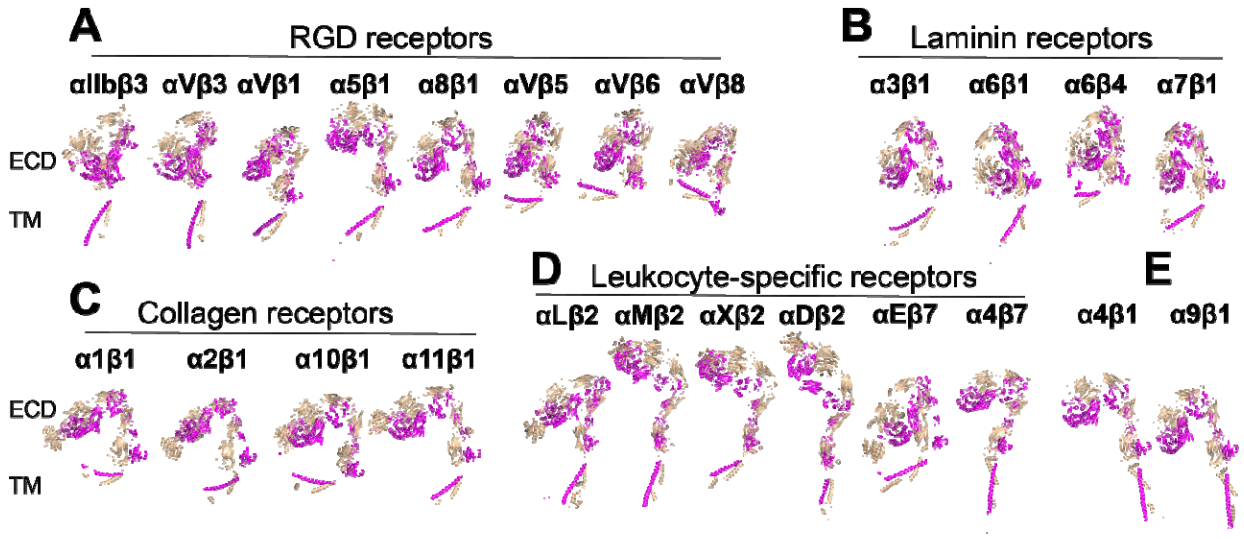

Figure 6. Structures of 24 human integrins predicted by AlphaFold2-multimer. (**A-E**) Full-length integrin structures were calculated using AlphaFold2-multimer with the max_template_date set to year 2000. Structures were superimposed onto the calf-2 domain of the α_{IIb} subunit and are presented in the same orientation. The α and β subunits are shown in wheat and magenta, respectively.

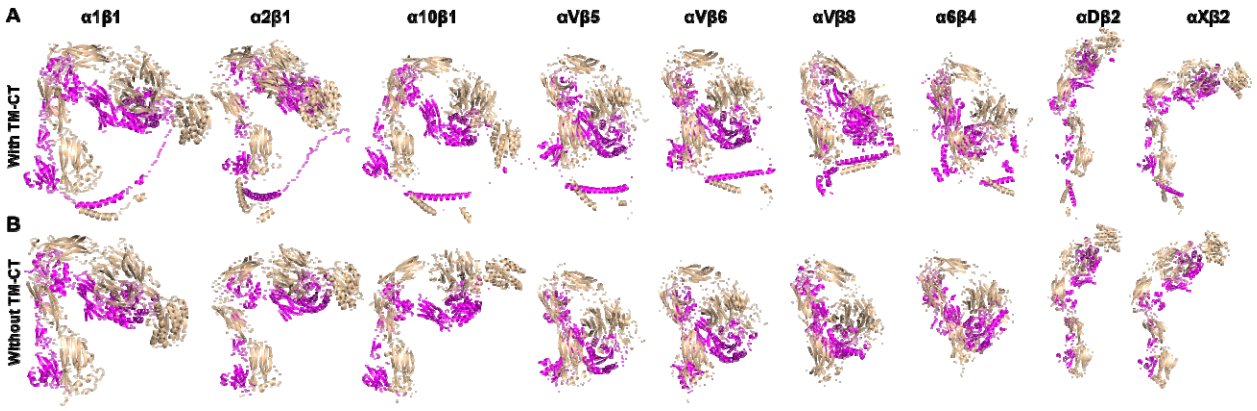

Figure 7. Comparison of structures predicted by AlphaFold2-multimer with and without transmembrane and cytoplasmic domains. (**A**) Full-length structures of certain integrins calculated by Alphafold2-multimer exhibit artificial contacts between the ectodomain and TM-CT domains. (**B**) The integrins shown in panel A were re-modeled by AlphaFold2-multimer in the absence of TM-CT domains. The structures were superimposed based on the calf-2 domain of the α subunit and are presented in the same orientation. The α and β subunits are shown in wheat and magenta, respectively.

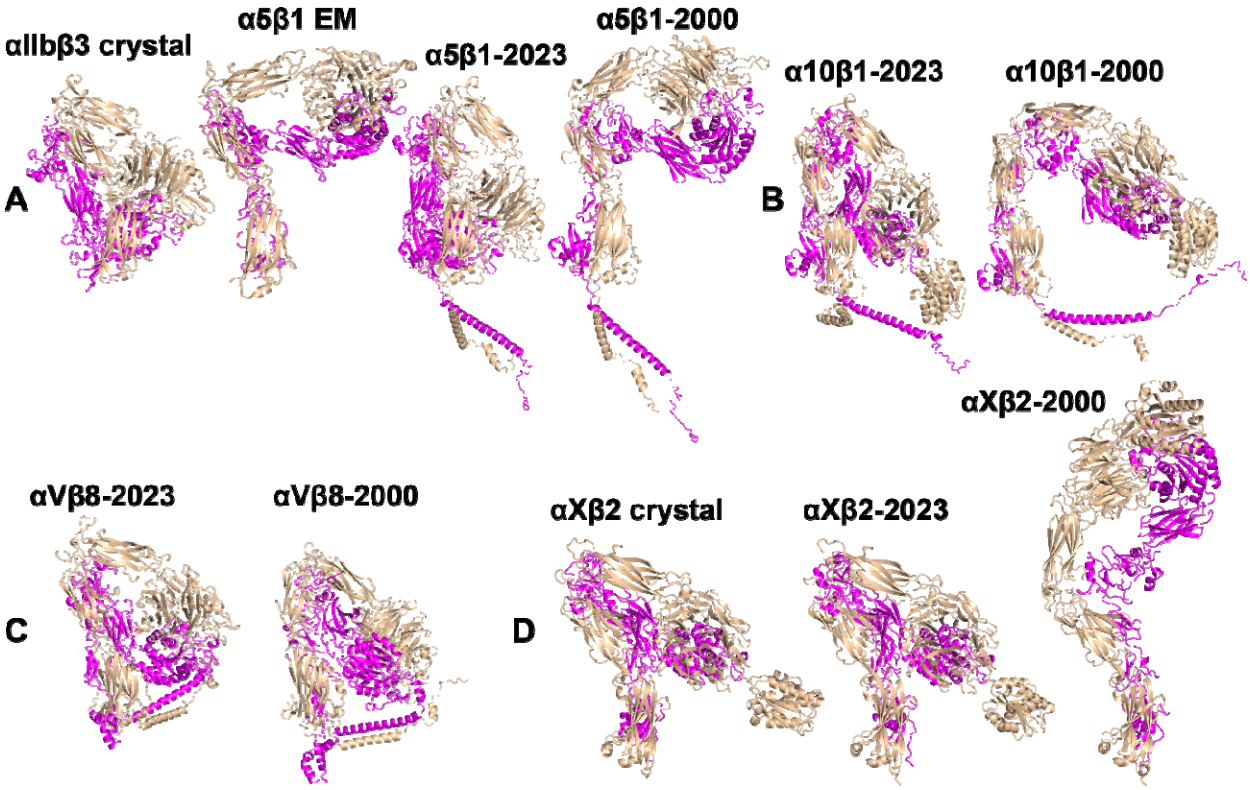

Figure 8. Comparison of selected structures predicted by AlphaFold2-multimer with and without enabling the option to use known structures as templates. (**A**) Full-length $\alpha_5\beta_1$ structures were calculated by AlphaFold2-multimer with the max_template_date set to either year 2023 or 2000. Crystal structure of $\alpha_{IIb}\beta_3$ (PDB 3FCS) and the cryo-EM structure of $\alpha_5\beta_1$ (PDB 7NXD) were provided for comparison. (**B**) AlphaFold2 structures of full-length $\alpha_{10}\beta_1$ with the max_template_date set to either year 2023 or 2000. (**C**) Full-length $\alpha_V\beta_8$ structures modeled by by AlphaFold2-multimer with the max_template_date set to either year 2023 or 2000. (**D**) AlphaFold2 structures of ectodomain of $\alpha_X\beta_2$. The crystal structure of $\alpha_X\beta_2$ (PDB 4NEH) was shown for comparison.

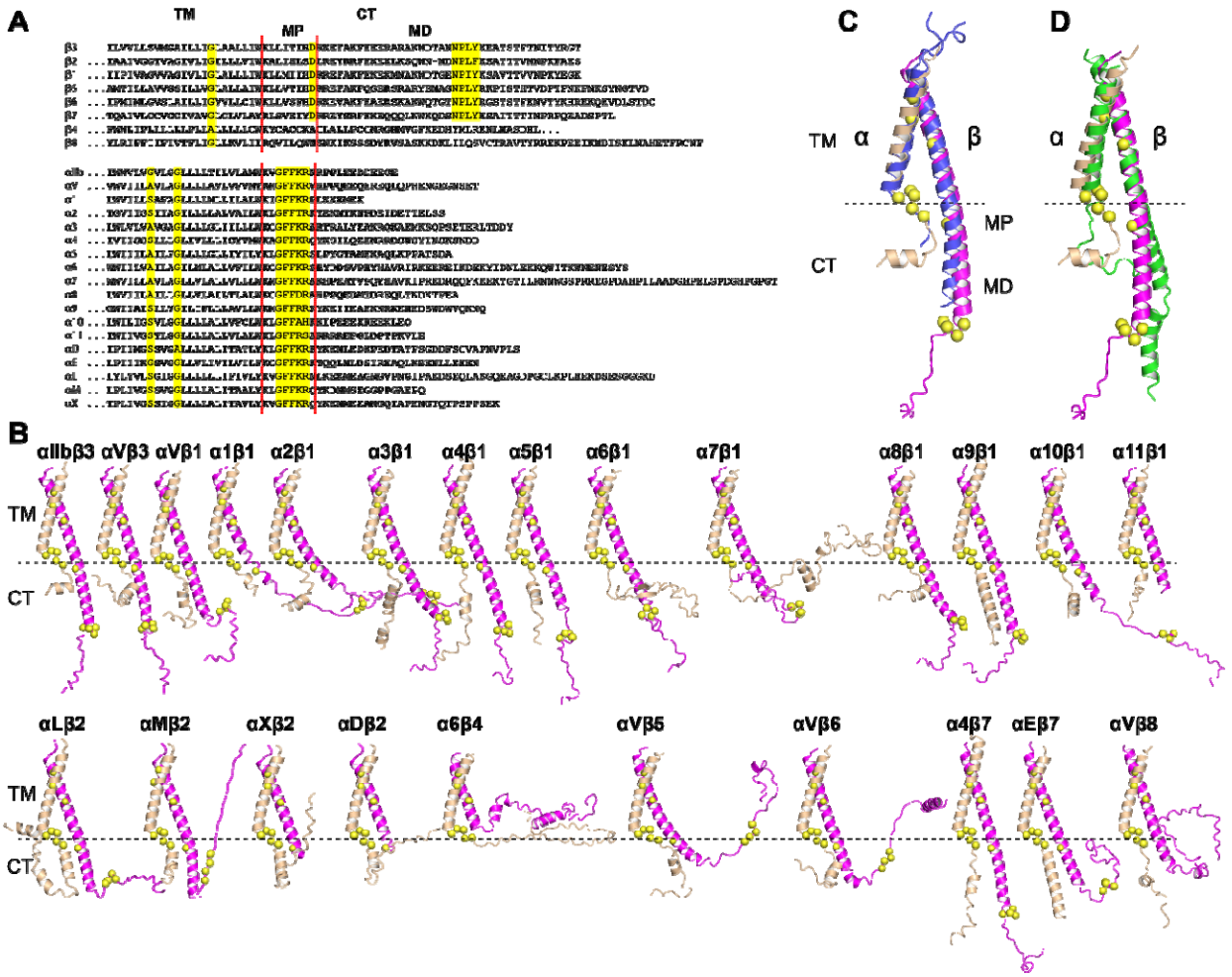

Figure 9. Structures of integrin transmembrane and cytoplasmic domains predicted by AlphaFold2-multimer. (**A**) Sequence alignment of human β and α integrin TM and CT domains. Conserved residues are highlighted in yellow. The boundaries of membrane proximal (MP) and membrane distal (MD) regions of CT domain are indicated. (**B**) AlphaFold2 structures of 24 human integrin TM-CT domains. The structures were superimposed onto the TM domain of α_{IIb} subunit and are presented in the same orientation. The conserved residues highlighted in panel A are depicted as yellow Cα spheres. (**C**) Superimposition of the AlphaFold2-predicted $\alpha_{IIb}\beta_3$ TM-CT structure (in wheat and magenta) onto the heterodimeric structure of $\alpha_{IIb}\beta_3$ TM-CT domains determined by disulfide crosslinking and Rosetta modeling (in blue). The α and β subunits are shown in wheat and magenta, respectively. (**D**) Superimposition of the $\alpha_{IIb}\beta_3$ TM-CT structure predicted without (green) and with (wheat and magenta) the ectodomain.

References

[1] Hynes, R. O. (2002) Integrins: bi-directional, allosteric, signalling machines, *Cell 110*, 673-687.

[2] Slack, R. J., Macdonald, S. J. F., Roper, J. A., Jenkins, R. G., and Hatley, R. J. D. (2022) Emerging therapeutic opportunities for integrin inhibitors, *Nat Rev Drug Discov 21*, 60-78.

[3] Ley, K., Rivera-Nieves, J., Sandborn, W. J., and Shattil, S. (2016) Integrin-based therapeutics: biological basis, clinical use and new drugs, *Nat Rev Drug Discov 15*, 173-183.

[4] Pang, X., He, X., Qiu, Z., Zhang, H., Xie, R., Liu, Z., Gu, Y., Zhao, N., Xiang, Q., and Cui, Y. (2023) Targeting integrin pathways: mechanisms and advances in therapy, *Signal Transduct Target Ther 8*, 1.

[5] Hynes, R. O., Ruoslahti, E., and Springer, T. A. (2022) Reflections on Integrins-Past, Present, and Future: The Albert Lasker Basic Medical Research Award, *JAMA 328*, 1291-1292.

[6] Springer, T. A., and Dustin, M. L. (2012) Integrin inside-out signaling and the immunological synapse, *Current opinion in cell biology 24*, 107-115.

[7] Luo, B.-H., Carman, C. V., and Springer, T. A. (2007) Structural basis of integrin regulation and signaling, *Annu. Rev. Imm. 25*, 619-647.

[8] Calderwood, D. A., Campbell, I. D., and Critchley, D. R. (2013) Talins and kindlins: partners in integrin-mediated adhesion, *Nature reviews. Molecular cell biology 14*, 503-517.

[9] Hu, P., and Luo, B. H. (2013) Integrin bi-directional signaling across the plasma membrane, *J Cell Physiol 228*, 306-312.

[10] Xiong, J.-P., Stehle, T., Diefenbach, B., Zhang, R., Dunker, R., Scott, D. L., Joachimiak, A., Goodman, S. L., and Arnaout, M. A. (2001) Crystal structure of the extracellular segment of integrin $\alpha_V\beta_3$, *Science 294*, 339-345.

[11] Xiong, J. P., Mahalingham, B., Alonso, J. L., Borrelli, L. A., Rui, X., Anand, S., Hyman, B. T., Rysiok, T., Muller-Pompalla, D., Goodman, S. L., and Arnaout, M. A. (2009) Crystal structure of the complete integrin $\alpha_V\beta_3$ ectodomain plus an α/β transmembrane fragment, *J Cell Biol 186*, 589-600.

[12] Dong, X., Mi, L.-Z., Zhu, J., Wang, W., Hu, P., Luo, B. H., and Springer, T. A. (2012) $\alpha_V\beta_3$ Integrin Crystal Structures and their Functional Implications, *Biochemistry 51*, 8814-8828.

[13] Xiao, T., Takagi, J., Wang, J.-h., Coller, B. S., and Springer, T. A. (2004) Structural basis for allostery in integrins and binding of fibrinogen-mimetic therapeutics, *Nature 432*, 59-67.

[14] Zhu, J., Luo, B. H., Xiao, T., Zhang, C., Nishida, N., and Springer, T. A. (2008) Structure of a complete integrin ectodomain in a physiologic resting state and activation and deactivation by applied forces, *Mol. Cell 32*, 849-861.

[15] Zhu, J., Zhu, J., Negri, A., Provasi, D., Filizola, M., Coller, B. S., and Springer, T. A. (2010) The closed headpiece of integrin $\alpha_{IIb}\beta_3$ and its complex with an $\alpha_{IIb}\beta_3$-specific antagonist that does not induce opening, *Blood 116*, 5050-5059.

[16] Zhu, J., Zhu, J., and Springer, T. A. (2013) Complete integrin headpiece opening in eight steps, *J Cell Biol 201*, 1053-1068.
[17] Thinn, A. M. M., Wang, Z., Zhou, D., Zhao, Y., Curtis, B. R., and Zhu, J. (2018) Autonomous conformational regulation of β_3 integrin and the conformation-dependent property of HPA-1a alloantibodies, *Proceedings of the National Academy of Sciences of the United States of America 115*, E9105-E9114.
[18] Zhou, D., Thinn, A. M. M., Zhao, Y., Wang, Z., and Zhu, J. (2018) Structure of an extended β_3 integrin, *Blood 132*, 962-972.
[19] Nesic, D., Zhang, Y., Spasic, A., Li, J., Provasi, D., Filizola, M., Walz, T., and Coller, B. S. (2020) Cryo-Electron Microscopy Structure of the $\alpha_{IIb}\beta_3$-Abciximab Complex, *Arteriosclerosis, thrombosis, and vascular biology 40*, 624-637.
[20] Adair, B. D., Xiong, J. P., Yeager, M., and Arnaout, M. A. (2023) Cryo-EM structures of full-length integrin alphaIIbbeta3 in native lipids, *Nat Commun 14*, 4168.
[21] Choi, W. S., Rice, W. J., Stokes, D. L., and Coller, B. S. (2013) Three-dimensional reconstruction of intact human integrin $\alpha_{IIb}\beta_3$: new implications for activation-dependent ligand binding, *Blood 122*, 4165-4171.
[22] Xia, W., and Springer, T. A. (2014) Metal ion and ligand binding of integrin $\alpha_5\beta_1$, *Proceedings of the National Academy of Sciences of the United States of America 111*, 17863-17868.
[23] Schumacher, S., Dedden, D., Nunez, R. V., Matoba, K., Takagi, J., Biertumpfel, C., and Mizuno, N. (2021) Structural insights into integrin $\alpha_5\beta_1$ opening by fibronectin ligand, *Sci Adv 7*.
[24] Nagae, M., Re, S., Mihara, E., Nogi, T., Sugita, Y., and Takagi, J. (2012) Crystal structure of $\alpha_5\beta_1$ integrin ectodomain: Atomic details of the fibronectin receptor, *J Cell Biol 197*, 131-140.
[25] Arimori, T., Miyazaki, N., Mihara, E., Takizawa, M., Taniguchi, Y., Cabanas, C., Sekiguchi, K., and Takagi, J. (2021) Structural mechanism of laminin recognition by integrin, *Nat Commun 12*, 4012.
[26] Sen, M., Yuki, K., and Springer, T. A. (2013) An internal ligand-bound, metastable state of a leukocyte integrin, $\alpha_X\beta_2$, *J Cell Biol 203*, 629-642.
[27] Xie, C., Zhu, J., Chen, X., Mi, L., Nishida, N., and Springer, T. A. (2010) Structure of an integrin with an αI domain, complement receptor type 4, *Embo J 29*, 666-679.
[28] Sen, M., and Springer, T. A. (2016) Leukocyte integrin $\alpha_L\beta_2$ headpiece structures: The alphaI domain, the pocket for the internal ligand, and concerted movements of its loops, *Proceedings of the National Academy of Sciences of the United States of America 113*, 2940-2945.
[29] Goldsmith, J. A., DiVenere, A. M., Maynard, J. A., and McLellan, J. S. (2022) Structural basis for non-canonical integrin engagement by Bordetella adenylate cyclase toxin, *Cell reports 40*, 111196.
[30] Jensen, R. K., Pedersen, H., Lorentzen, J., Laursen, N. S., Vorup-Jensen, T., and Andersen, G. R. (2022) Structural insights into the function-modulating effects of nanobody binding to the integrin receptor $\alpha_M\beta_2$, *J Biol Chem 298*, 102168.

[31] Dong, X., Zhao, B., Iacob, R. E., Zhu, J., Koksal, A. C., Lu, C., Engen, J. R., and Springer, T. A. (2017) Force interacts with macromolecular structure in activation of TGF-beta, *Nature 542*, 55-59.
[32] Dong, X., Hudson, N. E., Lu, C., and Springer, T. A. (2014) Structural determinants of integrin β-subunit specificity for latent TGF-beta, *Nat Struct Mol Biol 21*, 1091-1096.
[33] Kotecha, A., Wang, Q., Dong, X., Ilca, S. L., Ondiviela, M., Zihe, R., Seago, J., Charleston, B., Fry, E. E., Abrescia, N. G. A., Springer, T. A., Huiskonen, J. T., and Stuart, D. I. (2017) Rules of engagement between $\alpha_V\beta_6$ integrin and foot-and-mouth disease virus, *Nat Commun 8*, 15408.
[34] Cormier, A., Campbell, M. G., Ito, S., Wu, S., Lou, J., Marks, J., Baron, J. L., Nishimura, S. L., and Cheng, Y. (2018) Cryo-EM structure of the $\alpha_V\beta_8$ integrin reveals a mechanism for stabilizing integrin extension, *Nat Struct Mol Biol*.
[35] Wang, J., Su, Y., Iacob, R. E., Engen, J. R., and Springer, T. A. (2019) General structural features that regulate integrin affinity revealed by atypical $\alpha_V\beta_8$, *Nat Commun 10*, 5481.
[36] Campbell, M. G., Cormier, A., Ito, S., Seed, R. I., Bondesson, A. J., Lou, J., Marks, J. D., Baron, J. L., Cheng, Y., and Nishimura, S. L. (2020) Cryo-EM Reveals Integrin-Mediated TGF-beta Activation without Release from Latent TGF-beta, *Cell 180*, 490-501 e416.
[37] Duan, Z., Lin, X., Wang, L., Zhen, Q., Jiang, Y., Chen, C., Yang, J., Lee, C. H., Qin, Y., Li, Y., Zhao, B., Wang, J., and Zhang, Z. (2022) Specificity of TGF-β1 signal designated by LRRC33 and integrin $\alpha_V\beta_8$, *Nat Commun 13*, 4988.
[38] Yu, Y., Zhu, J., Mi, L. Z., Walz, T., Sun, H., Chen, J.-F., and Springer, T. A. (2012) Structural specializations of $\alpha_4\beta_7$, an integrin that mediates rolling adhesion, *J Cell Biol 196*, 131-146.
[39] Yang, J., Ma, Y. Q., Page, R. C., Misra, S., Plow, E. F., and Qin, J. (2009) Structure of an integrin $\alpha_{IIb}\beta_3$ transmembrane-cytoplasmic heterocomplex provides insight into integrin activation, *Proceedings of the National Academy of Sciences of the United States of America 106*, 17729-17734.
[40] Lau, T. L., Kim, C., Ginsberg, M. H., and Ulmer, T. S. (2009) The structure of the integrin $\alpha_{IIb}\beta_3$ transmembrane complex explains integrin transmembrane signalling, *Embo J 9*, 1351-1361.
[41] Zhu, J., Luo, B. H., Barth, P., Schonbrun, J., Baker, D., and Springer, T. A. (2009) The structure of a receptor with two associating transmembrane domains on the cell surface: integrin $\alpha_{IIb}\beta_3$, *Mol. Cell 34*, 234-249.
[42] Vinogradova, O., Velyvis, A., Velyviene, A., Hu, B., Haas, T. A., Plow, E. F., and Qin, J. (2002) A structural mechanism of integrin $\alpha_{IIb}\beta_3$ "inside-out" activation as regulated by its cytoplasmic face, *Cell 110*, 587-597.
[43] Weljie, A. M., Hwang, P. M., and Vogel, H. J. (2002) Solution structures of the cytoplasmic tail complex from platelet α_{IIb}- and β_3-subunits, *Proc. Natl. Acad. Sci. USA 99*, 5878-5883.
[44] Jumper, J., Evans, R., Pritzel, A., Green, T., Figurnov, M., Ronneberger, O., Tunyasuvunakool, K., Bates, R., Zidek, A., Potapenko, A., Bridgland, A., Meyer, C., Kohl, S. A. A., Ballard, A. J., Cowie, A., Romera-Paredes, B., Nikolov, S., Jain, R., Adler, J., Back, T., Petersen, S., Reiman, D., Clancy, E., Zielinski, M.,

Steinegger, M., Pacholska, M., Berghammer, T., Bodenstein, S., Silver, D., Vinyals, O., Senior, A. W., Kavukcuoglu, K., Kohli, P., and Hassabis, D. (2021) Highly accurate protein structure prediction with AlphaFold, *Nature 596*, 583-589.

[45] Evans, R., O'Neill, M., Pritzel, A., Antropova, N., Senior, A., Green, T., Žídek, A., Bates, R., Blackwell, S., Yim, J., Ronneberger, O., Bodenstein, S., Zielinski, M., Bridgland, A., Potapenko, A., Cowie, A., Tunyasuvunakool, K., Jain, R., Clancy, E., Kohli, P., Jumper, J., and Hassabis, D. (2022) Protein complex prediction with AlphaFold-Multimer, *bioRxiv*, 2021.2010.2004.463034.

[46] Laukaitis, C. M., Webb, D. J., Donais, K., and Horwitz, A. F. (2001) Differential dynamics of α_5 integrin, paxillin, and α-actinin during formation and disassembly of adhesions in migrating cells, *J Cell Biol 153*, 1427-1440.

[47] Wang, Z., and Zhu, J. (2021) Measurement of Integrin Activation and Conformational Changes on the Cell Surface by Soluble Ligand and Antibody Binding Assays, *Methods Mol Biol 2217*, 3-15.

[48] Smagghe, B., Huang, P., Ban, Y.-E., Baker, D., and Springer, T. A. (2010) Modulation of integrin activation by an entropic spring in the β-knee, *J Biol Chem 285*, 32954-32966.

[49] Askari, J. A., Tynan, C. J., Webb, S. E., Martin-Fernandez, M. L., Ballestrem, C., and Humphries, M. J. (2010) Focal adhesions are sites of integrin extension, *J Cell Biol 188*, 891-903.

[50] Hughes, P. E., Diaz-Gonzalez, F., Leong, L., Wu, C., McDonald, J. A., Shattil, S. J., and Ginsberg, M. H. (1996) Breaking the integrin hinge, *J. Biol. Chem. 271*, 6571-6574.

[51] Yin, R., Feng, B. Y., Varshney, A., and Pierce, B. G. (2022) Benchmarking AlphaFold for protein complex modeling reveals accuracy determinants, *Protein Sci 31*, e4379.

[52] Ibrahim, T., Khandare, V., Mirkin, F. G., Tumtas, Y., Bubeck, D., and Bozkurt, T. O. (2023) AlphaFold2-multimer guided high-accuracy prediction of typical and atypical ATG8-binding motifs, *PLoS Biol 21*, e3001962.